Supporting Information: Six-wave mixing induced by free-carrier plasma in silicon nanowire waveguides

Heng Zhou[1,*], Mingle Liao[1], Shu-Wei Huang[2], Linjie Zhou[3], Kun Qiu[1] and Chee Wei Wong[2,*]

[1] Key Lab of Optical Fiber Sensing and Communication Networks, University of Electronic Science and Technology of China, Chengdu 611731, China.

[2] Mesoscopic Optics and Quantum Electronics Laboratory, University of California, Los Angeles, CA 90095, USA.

[3] State Key Laboratory of Advanced Optical Communication Systems and Networks, Shanghai Jiao Tong University, Shanghai 200240, China.

[*]Corresponding author: zhouheng@uestc.edu.cn; cheewei.wong@ucla.edu

I. Configuration of the experimental measurements

In this study we examine six-wave mixing caused by the effective $\chi^{(5)}$ free-carrier plasma nonlinear dynamics. To demonstrate six-wave mixing, the most intuitive way is to apply five different input frequencies and reveal the non-degenerate wave mixing sidebands. However, as discussed in the main text, FC-SWM and FWM concurrently takes place in silicon nanowire; and a six-wave mixing process can always be decomposed into two cascaded four-wave mixing processes [R1]. In other words, the sideband frequencies generated by FC-SWM are always overlapped with cascaded FWMs – thus we cannot distinguish them simply by sideband frequencies [R2]. On such basis, in this Letter we utilized a two-laser experiment configuration to study degenerate FWM and degenerate FC-SWM processes (as shown in Fig. S1), and unambiguously demonstrate the existence of FC-SWM by discovering the regime where FC-SWM sufficiently prevails over FWM, caused intrinsically by the direct detuning dependence of FC-SWM, as shown in Fig. 2 of the main text. Furthermore, such compact and efficient experiment configuration also greatly simplifies the theoretical derivation towards the concise expressions of wave mixing sideband coefficients shown in Eq. (5-7) of the main text, which greatly facilitates our analysis of this nonlinear phenomenon.

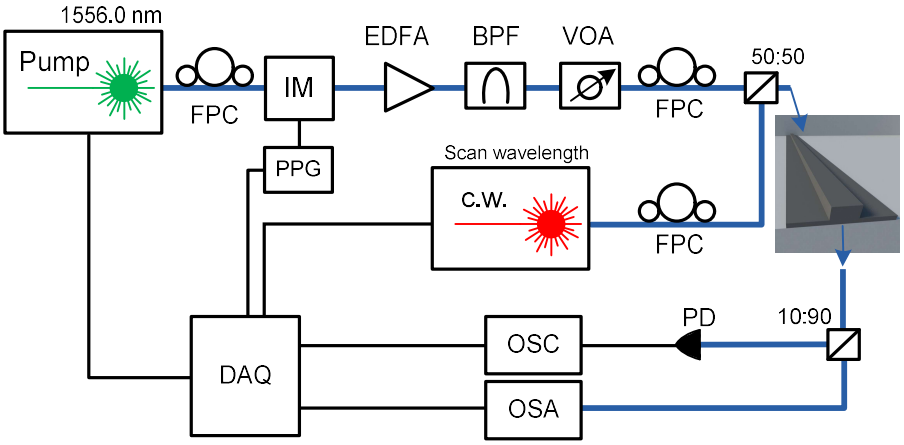

FIG. S1. Schematics of the experiment setup. FPC: fiber polarization controller, IM: intensity modulator; PPG: pulse-pattern generator; EDFA: erbium-doped fiber amplifier; BPF: band-pass filtering; VOA: variable optical attenuator; PD: photon diode; OSC: Oscilloscope; OSA: optical spectrum analyzer; and DAQ: data acquisition.

II. Derivation of the nonlinear modulation coefficient

The nonlinear field dynamics in the silicon nanowire is described by the nonlinear Schrödinger equation (NLSE) coupled with the rate equation of the intra-nanowire free-carrier density $N_c(z, t)$, given by [R3-R5]:

$$\frac{\partial E}{\partial z}=-i\frac{\beta_2}{2}\frac{\partial^2 E}{\partial t^2}+\frac{\beta_3}{6}\frac{\partial^3 E}{\partial t^3}-\frac{\alpha_l}{2}E+(i\gamma_{eff}-\frac{\beta_{TPA}}{2A_0})|E|^2E-(i\delta+\sigma)N_cE \tag{S1}$$

$$N_c(z,t)=\int_0^t\left(\frac{\beta_{TPA}}{2A_0^2h\nu_0}|E(z,\tau)|^4-\frac{N_c(z,\tau)}{\tau_c}\right)d\tau \tag{S2}$$

In Eq. (S1-S2), E is the slowly-varying envelope of the intra-nanowire electromagnetic fields, β_n is the nth order dispersion, α_l is the linear loss, γ_{eff} is the effective Kerr nonlinear coefficient, β_{TPA} is the degenerate two-photon absorption (TPA) coefficient, δ and σ is the free-carrier dispersion (FCD) and free-carrier absorption (FCA) coefficient respectively, A_0 is the effective mode area, and τ_c is the free-carrier lifetime. $N_c(z, t)$ is the free-carrier density with explicit z- and t-dependences shown for clarity. To study the wave mixing processes, we assume that, without loss of generality, an incident light field onto the silicon nanowire as $E = A_1\cos(\omega_1 t) + A_2\cos(\omega_2 t)$. To facilitate comparison with our measurements, here A_1 is a quasi-square pulse envelope with pulsewidth at half-maximum equal to T_o, and $A_1 \gg A_2$.

Examining the evolution of the overall input fields and neglecting the small nanowire dispersion, the nonlinear modulation term (*NM*) experienced by the input fields in the nanowire can be described by:

$$NM = \exp\left(L\left(i\gamma_{eff} - \frac{\beta_{TPA}}{2A_0} \right)|E|^2 - \frac{L(i\delta+\sigma)\beta_{TPA}}{2A_0^2 h\nu_0}\int_0^t |E|^4\, dt \right) \tag{S3}$$

Here L is the nanowire length. In Eq. (S3) we neglect free-carrier recombination relaxation since it is much slower (~ ns to 250 ps) than the beating oscillations considered in our study ($2\pi\tau_c \gg (\omega_1\text{-}\omega_2)^{-1}$). With the slow-varying envelope approximation [R1], we can neglect those fast oscillations at frequencies ω_1 , ω_2 , as well as their summation and multiples. Hence one obtains:

$$|E|^2 \to \frac{A_1^2}{2} + A_1 A_2 \cos(\omega_1 t - \omega_2 t) \tag{S4}$$

$$\begin{aligned} |E|^4 &\to A_1^4 \cos^4(\omega_1 t) + 4A_1^3 A_2 \cos^3(\omega_1 t)\cos(\omega_2 t) \\ &\to \frac{3A_1^4}{8} + \frac{3A_1^3 A_2}{2}\cos(\omega_1 t - \omega_2 t) \end{aligned} \tag{S5}$$

In the above derivation we use the condition that $A_1 \gg A_2$, relevant for our measurements, and neglect the terms containing A_2^2 . Considering that *NM* eventually applies on the high power pulse field $A_1\cos(\omega_1 t)$, Eq. (S4) represents the four-wave mixing process $\chi^{(3)}$($2\omega_1 - \omega_2; \omega_1, \omega_1, \omega_2$) and Eq. (5) represents the six-wave mixing process $\chi_{\mathrm{FC}}^{(5)}$ ($2\omega_1 - \omega_2; \omega_1, \omega_1, -\omega_1, \omega_1, \omega_2$). It is seen that under our experimental configuration, particular wave interactions are different for four- and six-wave mixing but both result in nonlinear modulation of frequency $\omega_1 - \omega_2$. Substituting Eq. (S4-S5) into Eq. (S3), we obtain:

$$NM = \exp\left(L\left(i\gamma_{eff} - \frac{\beta_{TPA}}{2A_0} \right)\left(\frac{A_1^2}{2} + A_1 A_2 \cos(bt) \right) - \frac{(i\delta+\sigma)\beta_{TPA} L}{2A_0^2 h\nu_0}\left(\frac{3A_1^4 T_0}{8} + \frac{3A_1^3 A_2}{2b}\sin(bt) \right) \right) \tag{S6}$$

where $b = \omega_1 - \omega_2$. To focus on the wave mixing processes, we eliminate the constant modulation terms in Eq. (S6) and keep only the oscillation terms to obtain:

$$NM = \exp\left((iG + P)\cos(bt) + \frac{(iD + A)}{b}\sin(bt) \right) \tag{S7}$$

Here $G = LA_1A_2\gamma_{eff}$, $P = -LA_1A_2\beta_{TPA}(2A_0)^{-1}$, $D = -3LA_1^3A_2\delta\beta_{TPA}(4A_0{}^2h\nu_0)^{-1}$, $A = D\sigma\delta^{-1}$. With our experimental parameters, we find that *G*, *P*, *D*, *A* are each substantially smaller than 1, such that Eq. (S3) is simplified to:

$$NM = \exp(iG\cos(bt) + \frac{iD}{b}\sin(bt)) \times (1 + P\cos(bt)) \times (1 + \frac{A}{b}\sin(bt)) \tag{S8}$$

Eq. (S8) can be further rearranged into the following form:

$$NM = \exp\left(iH\sin(bt+\theta)\right) \times \left(1 + M\cos(bt+\psi)\right) \tag{S9}$$

where $H = \sqrt{(D/b)^2 + G^2}$, $M = \sqrt{(A/b)^2 + P^2}$,with $\theta = \arctan\left(Gb/D\right)$, $\pi/2 \le \theta < \pi$, and $\psi = \arctan(-A/Pb)$, $\pi/2 \le \psi < \pi$. The values of θ and ψ are determined by the signs of *G*, *P*, *D*, and *A*. Using the Bessel expansion and Euler's formula, we obtain:

$$NM = \sum_{n=-1}^{1} J_n(H) e^{inbt+in\theta} \times \left(1 + \frac{1}{2}M\left(e^{ibt+i\psi} + e^{-ibt-i\psi}\right)\right) . \tag{S10}$$

Here J_n is the *n*th order Bessel function. In Eq. (S10) we note that the only possible values of *n* are -1, 0, and 1 because phase-matching condition cannot be satisfied for higher eigenfrequencies as confirmed in in the measurements. Subsequently, the nonlinear modulation terms at opposite detunings ±*b* are:

$$NM_b = \frac{1}{2}MJ_0e^{i\psi} + J_1e^{i\theta} \tag{S11}$$

$$NM_{-b} = \frac{1}{2}MJ_0e^{-i\psi} - J_1e^{-i\theta} \tag{S12}$$

In the above derivation we used $J_{-1} = -J_1$.

III. Deriving the interactions between different nonlinear six-wave and four-wave mixing effects

Below is the detailed derivation of Table I in the main text, based on Eq. (S11-S12).

i. when only Kerr and TPA are applied, *A=0*, *D*=0, $\theta = \pi/2$, $\psi = \pi$, $NM_b = -MJ_0/2 + iJ_1$; $NM_{-b} = -MJ_0/2 + iJ_1$.

ii. when only TPA and FCA are applied, *D=0*, *G*=0, $NM_b = Me^{i\varphi}/2$; $NM_{-b} = Me^{-i\varphi}/2$.

iii. when only Kerr and FCD are applied, *A=0*, *P*=0, $NM_b = J_1e^{i\theta}$; $NM_{-b} = -J_1e^{-i\theta}$.

iv. when only FCA and FCD are applied, *G=0*, *P*=0, $\theta = \pi$, $\psi = 3\pi/2$, $NM_b = iMJ_0/2 - J_1$; $NM_{-b} = -MJ_0/2 + J_1$.

v. when only Kerr and FCA are applied, $P=0$, $D=0$, $\theta=\pi/2$, $\psi=3\pi/2$, $NM_b=iMJ_0/2+iJ_1$; $NM_{-b}=-iMJ_0/2+iJ_1$.

vi. when only FCD and TPA are applied, $G=0$, $A=0$, $\theta=\pi$, $\psi=\pi$, $NM_b=-MJ_0/2-J_1$; $NM_{-b}=-MJ_0/2+J_1$.

IV. Comparing the analytical results with experimental and numerical results

To connect Eq. (S11-S12) with the experimental results shown in Fig. 1 in the main text, the wave mixing sideband s_1 generated at ω_1-b corresponds to NM_b [S5], and its power can be written as:

$$P_{s1}=\left|\left(\frac{1}{2}MJ_0e^{i\psi}+J_1e^{i\theta}\right)A_1\right|^2 \tag{S13}$$

Similarly, the wave mixing sideband s_2 generated at ω_1+b corresponds to NM_{-b}, and its power can be written as:

$$P_{s2}=\left|\left(\frac{1}{2}MJ_0e^{-i\psi}-J_1e^{-i\theta}\right)A_1\right|^2 \tag{S14}$$

In deriving of the above equations, we neglected nanowire dispersion and the time-independent nonlinear phase-shift induced by Kerr SPM, XPM, and FCD, which can in turn cause phase mismatch and reduce the sideband generation in the wave mixing process. However, we note that: i) the nanowire dispersion is comparatively negligibly small in our study; and ii) the overall phase mismatch caused by the nonlinear phase shift is independent of detuning. Therefore, there is only a constant discrepancy (~ 4 dB) between the sideband powers predicted by Eq. (S13-S14) and the experimental sideband measurements (and numerical simulated sideband powers). Correcting for this constant offset, the analytical results are nicely in line with simulations and experiments, as shown in Fig. 2 and Fig. 4 of the main text. Also, Fig. in the main text compares the numerical and analytical results induced by each combination of nonlinear wave mixing effects as listed in Table I in the main text, all exhibiting favorable agreement with each other.

V. Coupled-mode equations containing FC-SWM

Here we derive the coupled-mode equations of wave mixing in the presence of FC-SWM, based on the configuration adopted in our experiment [R6-R8]. Substituting the overall intra-nanowire field $E=E_1+E_2+E_3=A_1\cos(\omega_1 t)+A_2\cos(\omega_2 t)+A_3\cos(\omega_3 t)$ into Eq. (S1-S2) and following the derivation of Eq. (S6), we obtain:

$$dE=\left(\begin{array}{l}\left(i\gamma_{eff}+\dfrac{\beta_{TPA}}{2A_0}\right)\left(\dfrac{A_1^{\,2}}{2}+A_1A_2\cos(bt)+A_1A_3\cos(bt)\right)\\+\dfrac{(i\delta+\sigma)\beta_{TPA}}{2A_0^2h\nu_0}\left(\dfrac{3A_1^4T_0}{8}+\dfrac{3A_1^3A_2}{2b}\sin(bt)+\dfrac{3A_1^3A_3}{2b}\sin(bt)\right)\times\dfrac{dz}{L}\end{array}\right)E \tag{S15}$$

Expanding Eq. (S15) and gathering the terms with eigenfrequency ω_1, ω_2 and $\omega_3=\omega_1-\omega_2$, we have:

$$\frac{dA_1}{dz}=\left(\left(i\gamma_{eff}+\frac{\beta_{TPA}}{2A_0}\right)\left|A_1\right|^2+\frac{3(i\delta+\sigma)\beta_{TPA}}{16A_0^2h\nu_0}\left|A_1\right|^4T_0\right)A_1 \tag{S16}$$

$$\frac{dA_2}{dz}=\left(i\gamma_{eff}+\frac{\beta_{TPA}}{2A_0}\right)2\left|A_1\right|^2A_2+\frac{3(i\delta+\sigma)\beta_{TPA}}{16A_0^2h\nu_0}\left(\left|A_1\right|^4T_0+\frac{2\left|A_1\right|^2A_1^2e^{-i\frac{\pi}{2}}}{b}\right)A_2 \tag{S17}$$

$$\frac{dA_3}{dz}=\left(i\gamma_{eff}+\frac{\beta_{TPA}}{2A_0}\right)\left(2\left|A_1\right|^2A_3+A_1^{\,2}A_2\right)+\frac{3(i\delta+\sigma)\beta_{TPA}}{16A_0^2h\nu_0}\left(\left(T_0\left|A_1\right|^4+\frac{2\left|A_1\right|^2A_1^2e^{-i\frac{\pi}{2}}}{b}\right)A_3+\frac{2\left|A_1\right|^4A_2e^{-i\frac{\pi}{2}}}{b}\right) \tag{S18}$$

Here, in the derivation, we use $A_1\gg A_2\gg A_3$. Qualitatively, the pulse field E_1 experiences self-induced Kerr SPM, TPA, FCA, and FCD. The continuous-wave field E_2 mainly experiences Kerr XPM and the cross-induced TPA, FCA, and FCD from E_1. The sideband field E_3 experiences XPM and the cross-induced TPA, FCA, and FCD from E_1. Additionally it acquires energy from E_1 and E_2 via FWM (4^{th} term in the RHS of Eq. (S18)) and FC-SWM (last term in the RHS of Eq. (S18)). The coupled-mode equation model illustrates the evolution of each wave participating in the wave mixing and, specifically it enables the modeling of the wave mixing phase matching dynamics, as described in the next Section.

VI. Phase matching consideration of FC-SWM

It can be seen from Eq. (S5) that the phase-matching condition for FC-SWM is $2\kappa_{\omega1}-\kappa_{\omega2}=\kappa_{\omega3}$, where $\kappa_{\omega i}$ is the propagation constant at wavelength ω_i. It is noted that although FC-SWM is a six-wave mixing processes, its phase-matching condition is identical with Kerr FWM, since we utilized the bichromatic laser input to study the degenerate FC-SWM ($\chi^{(5)}(\,2\omega_1-\omega_2;\omega_1,\omega_1,-\omega_1,\omega_1,\omega_2)$) and FWM ($\chi^{(3)}(\,2\omega_1-\omega_2;\omega_1,\omega_1,\omega_2)$) [R9-R10]. From Eq. (S16-S18), the phase mismatch can be written as:

$$\Delta\kappa=2\kappa_{\omega1}-\kappa_{\omega2}-\kappa_{\omega3}=\Delta\phi-2\gamma_{eff}\left|A_1\right|^2 \tag{S19}$$

where $\Delta\phi$ denotes dispersion induced linear phase mismatch and $2\gamma_{eff}|A_1|^2$ denotes nonlinear phase mismatch caused by Kerr phase modulation. We emphasize that, as seen from Eq. (S16-S18), FCD causes large but identical nonlinear phase shift to all the intra-nanowire fields (as confirmed by the prominent spectral blue-shift and broadening of the pulse, c.w., and sideband spectrum shown in Fig. 1(b) of the main text), such that FCD does not contribute to the overall phase mismatch [R4, R11-R12]. Moreover, Fig. S2 shows the evolution of $\Delta\kappa\times L$ and the analytically calculated sideband power as the function of input laser wavelength detuning. We see that the peak value of $\Delta\kappa\times L$ is small (~ 0.34π), implying that the experimentally demonstrated wave mixing operates close to phase matching condition. In addition, for the experimental nanowire as noted in the main text, the influence of the detuning dependent phase mismatch caused by dispersion ($\Delta\phi \times L \sim 0.0041\pi$) is substantially weaker than the intrinsic $1/b$ scaling of FC-SWM.

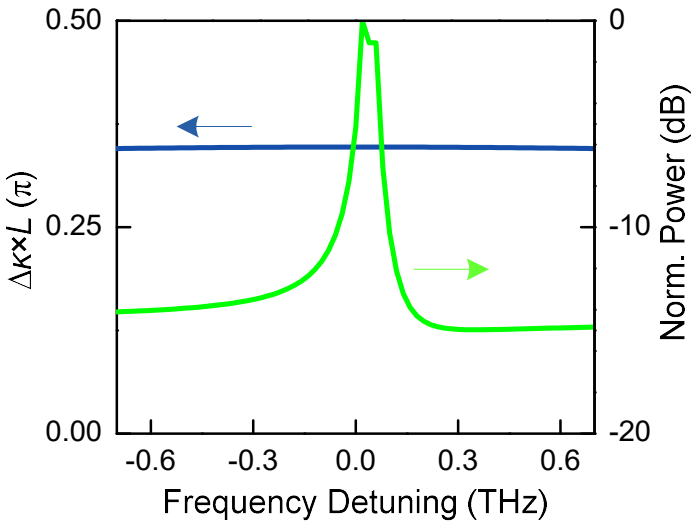

FIG. S2. Evolution of phase mismatch (left *y*-axis) and the analytically calculated normalized sideband power (right *y*-axis) as a function of input laser frequency detuning.

Supplementary References

[R1] M. Erkintalo, Y. Q. Xu, S. G. Murdoch, J. M. Dudley, and G. Genty, "Cascaded phase matching and nonlinear symmetry breaking in fiber frequency combs," *Phys. Rev. Lett.* **109**, 223904 (2012).

[R2] Y. P. Zhang, U. Khadka, B. Anderson, M. Xiao, "Temporal and spatial interference between four-wave mixing and six-wave mixing channels," *Phys. Rev. Lett*. **102**, 013601 (2009).

[R3] X. Yang and C. W. Wong, "Coupled-mode theory for stimulated Raman scattering in high-Q/V_m silicon photonic band gap defect cavity lasers", *Opt. Express* **15**, 4763 (2007).

[R4] A. B. Redondo, C. A. Husko, D. Eades, Y. Zhang, J. Li, T. F. Krauss, and B. J. Eggleton, "Observation of soliton compression in silicon photonic crystals", *Nat. Commun.* **5**, 3160 (2014).

[R5] L. Yin and G. P. Agrawal, "Impact of two-photon absorption on self-phase modulation in silicon waveguides", *Opt. Lett.* **32**, 2031 (2007).

[R6] H. A. Haus, *Waves and fields in optoelectronics*, Prentice Hall, Englewood Cliffs, New Jersey, 1st edition, 1984.

[R7] G. P. Agrawal, *Nonlinear Fiber Optics*, Academic Press, New York, New York, 3rd edition, 2001.

[R8] Q. Lin, O. J. Painter, and G. P. Agrawal, "Nonlinear optical phenomena in silicon waveguides: Modeling and applications," *Opt. Express* **15**, 16604 (2007).

[R9] Q. Lin., J. Zhang, P. M. Fauchet, and G. P. Agrawal, "Ultrabroadband parametric generation and wavelength conversion in silicon waveguides", *Opt. Express* **14**, 4786 (2006).

[R10] D. Dimitropoulos, V. Raghunathan, R. Claps, and B. Jalali, "Phase-matching and nonlinear optical processes in silicon waveguides", *Opt. Express* **12**, 149 (2003).

[R11] C. Monat, B. Corcoran, D. Pudo, M. Heidari, C. Grillet, M. D. Pelusi, D. J. Moss, B. J. Eggleton, T. P. White, L. O'Faolain, and T. F. Krauss, "Slow light enhanced nonlinear optics in silicon photonic crystal waveguides", *IEEE J. Sel. Topics Quantum Electron.* **16**, 344 (2010).

[R12] S. Roy, A. Marini, and F. Biancalana, "Self-frequency blueshift of dissipative solitons in silicon-based waveguides", *Phys. Rev. A* **87**, 065803 (2013).